KECK Geology Consortium
Learning Science Through Research
Published by the Keck Geology Consortium

Short Contributions
Keck Geology Consortium
Volume 37
May 2025
doi: 10.18277/AKRSG.2025.37.03

A REVISED MODEL FOR THE INITIATION OF CIRCUMFERENTIAL FAULTING ON ALBA MONS, MARS

DEMI DURHAM, Trinity University
Project Advisor: Benjamin Surpless

INTRODUCTION

Exploring the geometry and long-term evolution of segmented normal fault systems is vital for seismic hazard assessment and natural resource development. Complex fault geometries are better preserved on Mars relative to Earth because of low rates of erosion and deposition on the red planet. In addition, newly available (2023), high-resolution (5 m/pixel) imagery of the Mars CTX Mosaic permits us to examine fully exposed fault networks in more detail than anywhere in the solar system.

The Martian volcano-tectonic complex Alba Mons is in the northern Tharsis region (e.g., Tanaka, 1990). With a North-South diameter of 1000 km and an East-West diameter of 1400 km, the volcano is larger than any volcano found on Earth (e.g., Öhman and McGovern, 2014) (Fig. 1). The volcanic complex features two lobes east and west of the central dome and displays very few graben within the summit area or on the flanks of the central volcano. The western lobe is much larger than the eastern lobe, extending more than 300 km to the west of the central dome (Ivanov and Head, 2006). Alba Fossae (fossae: long, narrow depressions or troughs) is a spectacularly exposed circumferential fault system that stretches along the western flank of Alba Mons (Fig. 1). Ivanov and Head (2006) suggest that most graben associated with Alba Fossae coincide with a slope break.

I investigate the characteristics of segmented normal faulting of the Alba Fossae circumferential fault network to shed light on the evolution of the system. The faulting spans several hundred kilometers along the western flank of the volcano, where faulting interacts with linear fault systems that extend northward and southward from the volcano (Fig. 1). Regional faulting evolved over four stages (e.g., Tanaka et al., 1989; Tanaka, 1990), beginning in the Early and Middle Noachian (3.92-3.85 Ga), with circumferential faulting focused in the third and fourth stages (Scott and Tanaka, 1980; Ohman and McGovern, 2014).

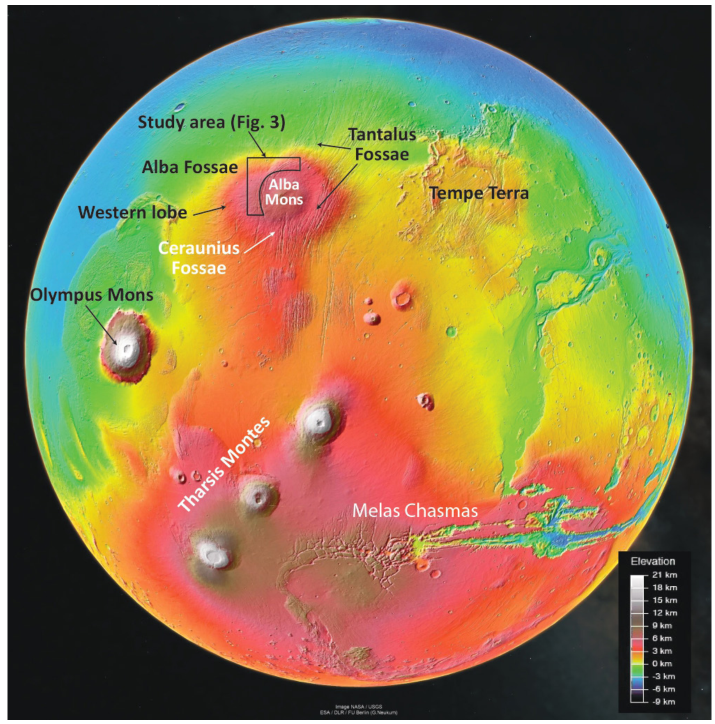

Figure 1. Colorized elevation overview of Mars. Note that the fault networks are labeled "fossae," the volcanoes are labeled "mons" or "montes," and the linear depressions are labeled "chasmas." (image from Google Earth/Mars, accessed 2024).

To analyze the fault network, I developed a workflow using Google Mars software. In Google Mars, I defined a series of sampling windows that capture different sections of the circumferential fault system to document fault system characteristics at different positions. I then used statistical analyses of fault characteristics to better understand the evolution of the system. Spatial variations in these characteristics allow us to relate changes in the local and regional stress fields and magnitudes of extension as faults propagated and accumulated displacement within the circumferential fault network.

BACKGROUND

Fault Segment Linkage

As fault segments propagate and accumulate displacement, they affect proximal stress fields, which can result in changes in strain distribution in the zone between faults (e.g., Crider and Pollard, 1998; Peacock, 2002). The geometries and spacing of segments influence whether and how linkage occurs; if spacing between two segments is too great, stress field interactions will not occur and faults will remain unlinked. However, if faults are more closely spaced, they may hard link and become segments of one single fault or may soft link by distributed strain (Fig. 2), which is commonly accommodated by a relay ramp (Peacock, 2002; McMillin, 2013; Taylor et al., 2024). Different fault displacements and geometries evolve based on whether the faults link before or after their tips overlap across strike (Fig. 2). En echelon normal fault systems of Alba Fossae display a wide range of linkage types.

Fault Development in the Northern Tharsis Region

Previous studies constrained four stages of faulting, from Noachian to Amazonian, across the northern Tharsis region, but the absolute ages of these stages are not precisely defined (Tanaka, 1989; 1990). Stage one of the region's structural evolution began in the Early Noachian (~4.1 Ga) and lasted through Late Noachian (3.92-3.85 Ga) time (Tanaka, 1989). These faults trended northeast, cut Noachian aged basement materials, and are related to plume tectonics centered at Tempe Terra (Tanaka et al., 1989; Tanaka, 1990). North-trending stage two faults like the Ceranius and Tantalus Fossae systems (Fig. 1) initiated in the Late Noachian through the Late Hesperian (3.85-1.8 Ga), cutting Noachian and Hesperian materials (Tanaka et

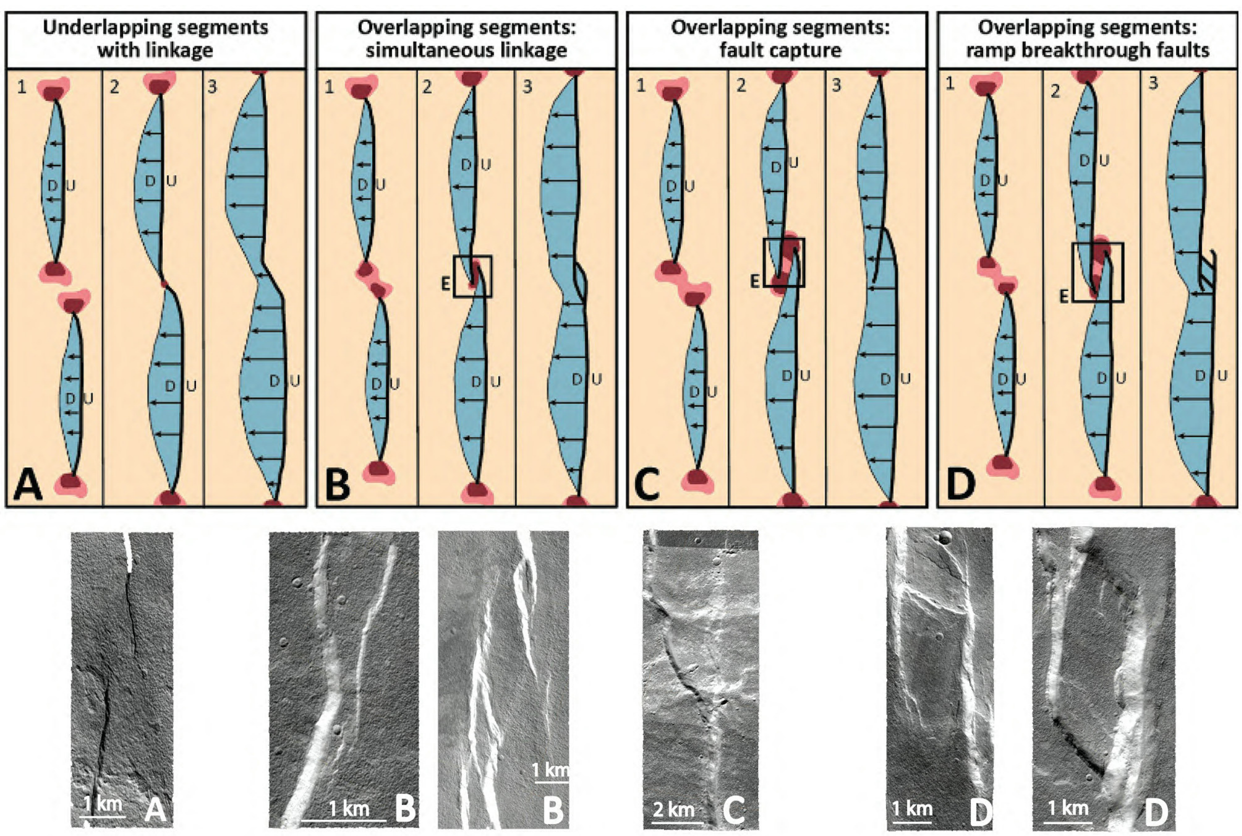

Figure 2. Diagrams displaying fault segment interactions, including stages of fault propagation and linkage, with stages 1-3 in chronological order (a-d). (modified from Taylor et al., 2024). Examples of fault segment interactions documented in the Alba Fossae fault system. Examples include: I) soft-linked underlap (between window C and D); II) soft-linked overlap (window C); III) complex overlap (window G); IV) fault capture (window A); V) Relay ramp base breach in window D; and VI) Relay ramp top and base breach (window C).

al., 1989). Faults from this stage crosscut stage one faults and remain active throughout subsequent stages (Tanaka, 1990).

Stage three of fault evolution in the Tharsis region may have begun with either a broad collapse of the volcanic dome of Alba Mons during the final stages of volcanism in Early Amazonian time (~1.8 Ga) (e.g., Tanaka 1989; 1990) or by doming and uplift of the volcano or some combination of the two mechanisms (e.g., Tanaka et al., 1989; Tanaka, 1990; McGovern et. al., 2001; Scott and Wilson, 2003; Ohman and McGovern, 2014). Tanaka et al. (1989) suggest that changes in the dome also resulted in intense faulting along faults of Ceranius Fossae to the south and in the plains north of Alba Mons (Fig. 1).

Stage four faults are discerned from stage three faults based on their linearity in the Tantalus Fossae and their narrow, sharp appearance in the Ceranius Fossae (Fig. 3; Tanaka, 1990). Structures in the fourth stage of development spanned from the early to late Amazonian (0.25 Gya) (Tanaka et al., 1989; Tanaka, 1990). Many stage four faults are likely a result of the reactivation or continued activity of buried faults from stages two and three (Tanaka et al., 1989; Tanaka, 1990; McMillin, 2013).

METHODS

I used Google Earth (Mars) to document fault characteristics and geometries in sampling windows B-H (Fig. 3). I measured segment lengths, linkage type (hard or soft linked), lateral overlap (the strike-parallel length of fault segment overlap), en echelon step direction, and fault offset (strike-perpendicular distance between two fault segments). Because faults in window A display significant interactions with faults from Tantalus Fossae over a ~250 km^2 area, I did not include them in this analysis. However, I do use interactions between fault networks exposed in window A when interpreting fault network evolution.

Based on map-view observations of sampling windows B-H (50 km eye altitude in Google Mars), I measured the average spacing perpendicular to fault strike across the fault network along a line of section approximately centered in each window (see Window E in Fig. 3, for example). Using the 200-m

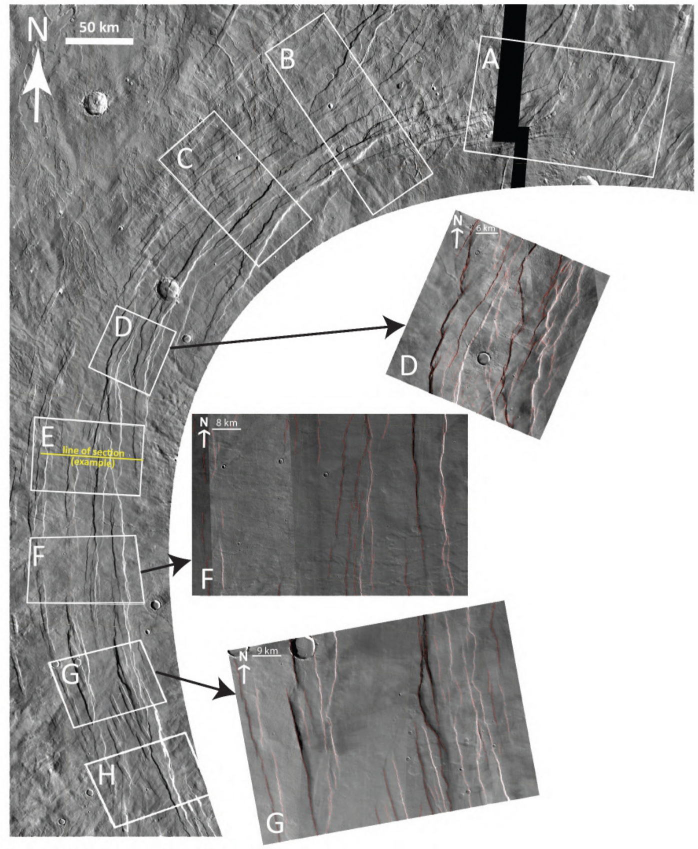

Figure 3. The Alba Fossae circumferential fault system (see Fig. 1) with outlines for windows A - H. Example of a line of section in window E. Sample window D) Red lines trace 708 documented segments, dominated by left-stepping en echelon geometries (Table 1). Sample window F) Red lines trace 308 documented segments with relatively short segment lengths (Table 1). Segments here are dominated by hard-linking geometries (Table 1). Sample window G) Red lines trace 261 documented segments with a strong right-stepping preference (Table 1). Window G has a large proportion of soft-linkages compared to the other sampling windows (Table 1).

DEM (based on the Mars Orbital Laser Altimetry mission, or MOLA), I was able to measure the vertical displacement (throw) for each of the major faults along each line of section. I then used the measured throw for each fault to calculate heave at each fault, assuming a dip of 60 degrees, which is typical for normal faults. By adding heave values, I was able to estimate total horizontal displacement, which I used to calculate extension in each study window.

Finally, to evaluate the hypothesis of Ivanov and Head (2006), who suggested that a slope break on the western lobe of Alba Mons had implications for the location of the circumferential fault system, I captured an elevation profile of the western lobe using Google Earth (Mars) to examine topography relative to the fault system.

RESULTS

Variations in Fault Geometries and Characteristics

The Amazonian and Hesperian volcanic unit that surrounds Alba Mons is composed of stacked, gently sloping lobate flows meters to tens of meters thick and hundreds of kilometers long (e.g., Tanaka, 2014). We confirmed that the circumferential fault system cuts this unit, which post-dates the first two stages outlined in Tanaka (1990). There is debate over the extent of Alba Fossae, with recent research positing that the system includes faults to the north of the circumferential system (Ivanov and Head, 2006; Wiedeking et al., 2023). However, our analysis of window A reveals that the faults of the circumferential system clearly cut and displace older, north trending faults of Tantalus Fossae at a high angle (Figs. 1 and 3).

To gain a better understanding of along-strike changes in the Alba Fossae system, I documented detailed fault characteristics for windows B through H (Table 1). The total extension accommodated is low for all windows, consistent with past studies of the fault system (e.g., Ohman and McGovern, 2014). My extension values ranged from 1.2-1.3% for windows C and D and from 0.3% to 0.8% for other windows (Table 1). Windows with the highest extension values correspond with the lowest average fault spacing (i.e., greatest cross-strike fault density), while the lowest extension values correspond with the highest average spacing (Table 1).

There is significant along-strike variability in how faults accommodate strain across the circumferential system. As an example, within Window C, there are two fault sets that accommodate extension with a 25 degree difference in strike, suggesting that strain is partitioned between the two sets. These sets also suggest a change in the stress field over time (e.g., Grant and Kattenhorn, 2004), with one set likely pre-dating the other, setting up a strong en echelon fabric along several major faults in Window C. Also interesting, there is a large graben system in the northernmost section of window G that terminates along strike to the north, with no significant equivalent structure in the southern section of window F to the north (Fig. 3).

Dominant linkage type transitions from soft- to hard-linked from windows B to D, with D having the most hard-linkages of all sampling windows. This could suggest an east-west dominant regional extension direction as opposed to northwest-southeast orientation suggested by previous studies (Caullieau et. al., 2003). Dominant linkage in windows E and G are mostly soft, while windows F and H display more hard linked segments. Both average segment length and strike-perpendicular offset distance are highest within the northernmost and southernmost windows, with shorter segments and offset distances in windows C through G (Table 1). The northernmost windows (B, C, and D) display a strong preference for left-stepping en echelon geometry, while southern windows (E, G, and H) display a right-step preference (Table 1). Window F displays no step preference (Table 1). In addition, en echelon stepovers are far more common in the northernmost windows (B, C, and D) compared to central and southern windows.

Influence of magmatic processes and pre-existing faults on Alba Fossae initiation and propagation

Ivanov and Head (2006) suggested that the initiation and propagation of Alba Fossae was affected by a break in slope on the western flank of Alba Mons (Ivanov and Head, 2006). However, the high resolution CTX images of Google Earth (Mars) and our DEM-based topographic profile from the western flank of Alba Mons shows that the fault system does not lie on the slope break but instead lies on the summit of the western lobe (Fig. 4). The coincidence of Alba Fossae with the summit of the western lobe (Fig. 4) suggests the possibility that magmatism played a role in the initiation of Alba Fossae (e.g., Hauber et al., 2010) and shows that the location of fault system initiation and propagation was not based on a topographic slope break.

The fact that there are no similar structures on the east flank likely means that the actual magnitude of uplift or subsidence may not have been significant enough to form faults around the dome. We suggest that dike injection and magmatic overpressure near the topographic high of the large western volcanic lobe may have concentrated the tensile stresses of the local stress field (e.g., Rubin and Pollard, 1988; Rivalta et al., 2015; Koehn et al., 2019) so that circumferential

Table 1. Sampling window fault characteristics.

Section	L_i (km)	L_f (km)	Heave (m)	Throw (m)	e	%e	Avg spacing (km)	Spacing SD
Window B	100.08	100.67	589	1020	0.006	0.6%	8.82	7.13
Window C	91.39	92.54	1146	1985	0.013	1.3%	3.75	1.67
Window D	39.36	39.84	473	819	0.012	1.2%	2.50	2.53
Window E	70.97	71.56	589	1020	0.008	0.8%	5.74	3.07
Window F	72.77	73.16	392	679	0.005	0.5%	5.84	4.77
Window G	56.83	57.24	401	694	0.007	0.7%	4.39	2.97
Window H	65.26	65.49	225	390	0.003	0.3%	7.70	6.35

Section	Segment Length (km)	Length SD	Offset (km)	Offset SD	Step Preference (left)	Dominant Linkage (hard)	Stepover Count
Window B	8.22	8.09	2.80	1.31	0.83	0.46	24
Window C	3.02	2.73	2.11	1.33	0.82	0.57	28
Window D	1.14	1.74	0.97	0.71	0.82	0.88	33
Window E	2.09	1.56	2.45	1.41	0.40	0.40	5
Window F	1.58	1.81	0.38	0.15	0.50	0.70	10
Window G	2.77	4.40	0.71	0.45	0.36	0.42	12
Window H	5.23	5.61	2.62	0.93	0.43	0.57	7

faulting associated with both magma injection and dome uplift or subsidence could have initiated there. There is evidence of a density increase in the mid and lower crust below the volcano likely formed a local stress field (Caullieau et. al., 2003). The local stress field would have been superposed on a regional stress field and might have been affected by volcanic activity (e.g., Caullieau et. al., 2003; Ohman and McGovern, 2014). This would suggest that the circumferential faulting was caused by a combination of long-term and short-term tectonic and intrusive processes. Cailleau et al. (2003) suggest that during the final stages of volcanic shield construction, the number of circumferential graben increased with a decrease in the feeding of the dome. We suggest that once faulting began near the western lobe summit, it was easier for lateral propagation to continue northward and southward along a path consistent with that of deformation related to dome inflation or deflation.

However, our data show that propagation of the circumferential fault system was likely affected by preexisting fault systems that trend approximately north-south at the northern (Tantalus Fossae) and southern (Ceranius Fossae) margins of Alba Mons. Fault segments in northern and southern windows exhibit right-stepping and left-stepping geometries, respectively. Thus, if Alba Fossae faulting first initiated near the summit of the western lobe and propagated north and south, it would have encountered the stress fields of pre-existing fault systems that affected the sense of en echelon step.

In addition to elucidating the genesis of the Alba Fossae system, the segment lengths and extension measurements in this study give us insight into the evolution and strain distribution of the fault network. The greatest segment lengths are associated with the greatest segment offset distances, consistent with stress-based arguments that greater offset distances make linking less likely, thus allowing faults to propagate further laterally without interacting with neighbors (e.g., Peacock, 2002). Although total finite extension across Alba Fossae is low (<1.5% for all windows), in map view, the windows with greater extension also exhibit the highest fault density, measured perpendicular to fault strike. This suggests the most faults along the Alba Fossae system

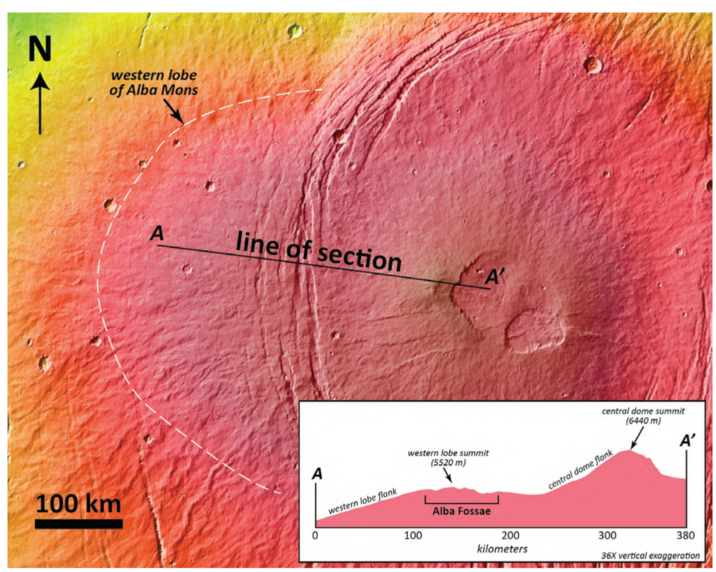

Figure 4. Colorized terrain of Alba Mons and elevation profile showing slope break.

accommodate similar finite extension.

Based on our analysis and previous research, we suggest the evolution of the Alba Fossae system is as follows:

● North-trending faults exposed north and south of the volcanic edifice propagated prior to significant volcanism of Alba Mons (Stage 2 of Tanaka, 1990)

● Extrusive volcanism occurs to build the volcanic edifice of Alba Mons. Near the end of magmatic activity, dome uplift or subsidence sets up a stress field consistent with circumferential faulting.

● Magmatic activity at the western lobe (magmatic overpressure during dike injections) makes it easier for graben structures to form at the summit of the western lobe. This would be an unlikely location for the graben to form if uplift or subsidence of the primary Alba Mons dome was the only factor in fault initiation and propagation.

● The graben propagated north and south of the summit dome and interact with faults north and south of the Alba Mons edifice, generating en echelon geometries along the northern and southern extents of the circumferential system.

● The ENE-striking circumferential fault system cross-cuts (post-dates) the north-striking faults of Tantalus Fossae within Window A (Fig. 3) so cannot be considered part of the same fault system, as hypothesized by Weideking et al. (2023).

ACKNOWLEDGEMENTS

This material is based upon work supported by the Keck Geology Consortium and the National Science Foundation under Grant No. 2050697. Funding for this project was provided by a 2024-2025 Keck Geology Consortium Advanced Research Project Grant as part of an NSF-REU Award to the Keck Geology Consortium (EAR 1659322; PIs Wirth, K., and Davidson, C.). Funding was also provided by NSF Award 2042114 to PI Surpless.

REFERENCES

Cailleau, B., Walter, T.R., Janle, P., and Hauber, E., 2003, Modeling volcanic deformation in a regional stress field: Implications for the formation of graben structures on Alba Patera, Mars: Journal of Geophysical Research: Planets, v. 108, doi: 10.1029/2003je002135.

Crider, J.G. and Pollard, D.D., 1998, Fault linkage: three-dimensional mechanical interaction between echelon normal faults: Journal of Geophysical Research, v. 103, p. 24,373-24,391.

Grant, J.V., and Kattenhorn, S.A., 2004, Evolution of vertical faults at an extensional plate boundary, southwest Iceland: Journal of Structural Geology, v. 26, p. 537-557.

Hauber, E., Grott, M., and Kronberg, P., 2010, Martian rifts: Structural geology and geophysics: Earth and Planetary Science Letters, v. 294, p. 393-410, https://doi.org/10.1016/j.epsl.2009.11.005.

Ivanov, M. A., & Head, J. W. (2006). Alba Patera, Mars: Topography, structure, and evolution of a unique late Hesperian–early Amazonian shield volcano. Journal of Geophysical Research, 111(E9). https://doi.org/10.1029/2005je002469

Koehn, D., A. Steiner, and K. Aanyu (2019), Modelling of extension and dyking-induced collapse faults and fissures in rifts, Journal of Structural Geology, 118, 21–31, doi: 10.1016/j.jsg.2018.09.017.

McGovern, P.J., Solomon, S.C., Head, J.W., Smith, D.E., Zuber, M.T., and Neumann, G.A., 2001, Extension and uplift at Alba Patera, Mars: Insights from mola observations and loading models: Journal of Geophysical Research: Planets, v. 106, p. 23769–23809, doi: 10.1029/2000je001314.

McMillin, A.M., 2013, Assessment of Linkage Likelihood in Segmented Normal Fault Systems in the Tharsis Region, Mars, [MS Thesis]: University of Alaska at Anchorage

Öhman, T., and McGovern, P. J., 2014, Circumferential graben and the structural evolution of Alba Mons, Mars. Icarus, 233, 114–125. https://-doi.org/10.1016/j.icarus.2014.01.043

Peacock, D., 2002, Propagation, interaction and linkage in normal fault systems: Earth-Science Reviews, vol. 58, nos. 1–2, p. 121–142.

Polit, A.T., Schultz, R.A., and Soliva, R., 2009, Geometry, displacement–length scaling, and extensional strain of normal faults on Mars with inferences on mechanical stratigraphy of the Martian crust: Journal of Structural Geology, v. 31, p. 662–673, doi: 10.1016/j.jsg.2009.03.016.

Rivalta, E., B. Taisne, A. P. Bunger, and R. F. Katz, 2015, A review of mechanical models of dike propagation: Schools of thought, results and future directions, Tectonophysics, v. 638, p. 1–42, doi: 10.1016/j.tecto.2014.10.003.

Rubin, A. M., and D. D. Pollard (1988), Dike-induced faulting in rift zones of iceland and afar, Geology, 16(5), 413, doi: 10.1130/0091-7613(1988)016<0413:difirz>2.3.co;2.

Scott, D.H., and Tanaka, K.L., 1980, in Lunar and Planetary Science Conference Proceedings, Houston, Pergamon Press, v. 3, p. 2403–2421.

Scott, E., and L. Wilson (2003), Did the Alba Patera and Syria Planum regions of Mars lose their lithospheric roots in convective overturn events? J. Geophys. Res., 108, 5035, doi:10.1029/2002JE001492, E5.

Tanaka, K.L., Davis, P.A., and Golombek, M.P., 1989, Development of grabens, tension cracks, and pits southeast of Albe Patera, Mars, In T.R. Watters and M.P. Golombek, Eds., MEVIV Workshop on Tectonic Features on Mars: LPI Technical Report 89-06, Lunar and Planetary Institute, Houston.

Tanaka, K.L., 1990, Tectonic History of the Alba Patera-Ceraunius Fossae Region of Mars, in Lunar and Planetary Science Conference Proceedings, Houston, TX, Branch of Astrogeology, US Geological Survey, p. 515–523.

Tanaka, K.L., 2014, The new geologic map of mars: Guiding research and education: Eos, Transactions American Geophysical Union, v. 95, p. 341–342, doi: 10.1002/2014eo380001.

Taylor, W., Surpless, B., Schiefelbein Kerscher, I., 2024, Complex Segment Linkage Along the Sevier Normal Fault, Southwestern Utah: Lithosphere, Special v. 15, doi: /10.2113/2024/lithosphere_2023_332.

Wiedeking, S., Lentz, A., Pasckert, J.H., Raack, J., Schmedemann, N., and Hiesinger, H., 2023, Rheological properties and ages of lava flows on Alba Mons, Mars: Icarus, v. 389, p. 115267, doi: 10.1016/j.icarus.2022.115267